

# Synthesis and Self-Assembly of Well-Defined Star and Tadpole Homo-/Co-/Terpolymers

George Polymeropoulos,<sup>†</sup> Panayiotis Bilalis,<sup>†</sup> Xueyan Feng,<sup>‡</sup> Edwin L. Thomas,<sup>\*,‡</sup> Yves Gnanou,<sup>§</sup> and Nikos Hadjichristidis<sup>\*,†</sup>

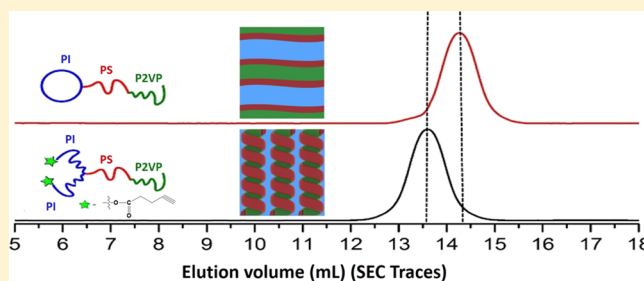
<sup>†</sup>Physical Sciences and Engineering Division, KAUST Catalysis Center, Polymer Synthesis Laboratory, King Abdullah University of Science and Technology (KAUST), Thuwal 23955, Saudi Arabia

<sup>‡</sup>Department of Materials Science and Nano-Engineering, Rice University, Houston, Texas 77030, United States

<sup>§</sup>Division of Physical Sciences & Engineering, King Abdullah University of Science and Technology (KAUST), Thuwal 23955, Saudi Arabia

## Supporting Information

**ABSTRACT:** Tadpole polymers are excellent candidates to explore how architecture can influence self-assembly because they combine two topologies in the same molecule (ring polymer as the head and linear polymer as the tail). In this work, we synthesize well-defined tadpole homo-/co-/terpolymers derived from the appropriate chemical modification reactions of the corresponding 3-miktoarm star homo-/co-/terpolymers via anionic polymerization, high vacuum techniques, and chlorosilane chemistry in combination with the Glaser coupling reaction. The 3-miktoarm star homo-/co-/terpolymers bear two arms with *t*-butyl dimethylsilyloxypropyl functional end-groups, whereas after deprotection, the  $\omega$ -hydroxyl chain-ends were modified to alkyne moieties. The dialkyne star polymers in the presence of Cu(I)Br and *N,N,N',N'',N'''*-pentamethyldiethylenetriamine were then transformed to well-defined tadpole homo-/co-/terpolymers. We employed strongly immiscible blocks to enable characterization using electron microscopy and X-ray scattering to explore how the molecular topology influences the self-assembled bulk-state microdomain morphologies.



## INTRODUCTION

The advent of “living” anionic polymerization<sup>1</sup> in the 1950’s enabled the synthesis of a broad portfolio of polymers with complex macromolecular architectures<sup>2</sup> such as star,<sup>3–6</sup> branched,<sup>7–11</sup> cyclic,<sup>12–14</sup> dendritic,<sup>15,16</sup> and graft<sup>17–19</sup> polymers and so forth. Considerable attention has been paid to the cyclic polymers because of their unique properties derived from the absence of chain-ends. It is well known that cyclic polymers possess smaller hydrodynamic volumes, higher glass transition temperatures, and lower intrinsic viscosities and consequently exhibit different properties compared to their linear/star analogues.<sup>20</sup> Among the two general strategies for synthesizing cyclic polymers, the ring expansion technique<sup>21,22</sup> affords the synthesis of high-purity, high molecular weight cyclic polymers but faces severe limitations concerning the variety of monomers that can be used, poor control over molecular weight, and broad polydispersity. On the other hand, the ring closure technique<sup>23,24</sup> is applicable to a great number of monomers and offers higher tolerance to different functional end-groups but has to overcome the entropic penalties associated with having the two chain-ends approach closely enough to bond.

Despite the above-mentioned limitations, the ring closure strategy has been widely used for the synthesis of a plethora of

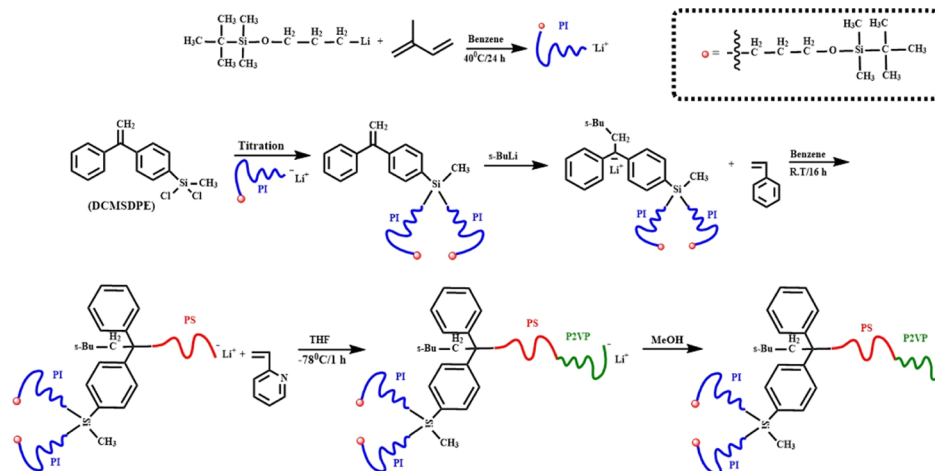
ring polymers such as cyclic homopolymers,<sup>25,26</sup> cyclic diblock copolymers,<sup>27,28</sup> and cyclic triblock terpolymers.<sup>29,30</sup> Most importantly, via the ring closure methodology, the synthesis of even more complex cyclic-based macromolecular architectures such as tadpole,<sup>31–33</sup> dicyclic,<sup>34,35</sup> multicycle,<sup>36,37</sup> eight-shaped,<sup>38,39</sup> and spiro-bicyclic polymers<sup>40,41</sup> was feasible. The lack of experimental data on the self-assembly of tadpole co-/terpolymers, arises from the inherent difficulties in synthesizing such chain architectures composed of blocks with large segment–segment interaction parameters and appropriate molecular weights to induce microphase separation. In our previous work,<sup>29</sup> the combination of anionic polymerization with the Glaser coupling reaction afforded the synthesis of well-defined cyclic triblock terpolymers consisting of polyisoprene (PI), polystyrene (PS), and poly(2-vinylpyridine) (P2VP). It was found out that the Glaser coupling reaction between terminal alkynes in the presence of Cu(I)Br and *N,N,N',N'',N'''*-pentamethyldiethylenetriamine (PMDETA), under high dilution, promotes the formation of 1,3-diyne rings in high yield, without the presence of polycondensation

Received: May 16, 2019

Revised: July 1, 2019

Published: July 17, 2019

Scheme 1. Synthetic Route of 3-Miktoarm Star Terpolymer Consisting of PI, PS, and P2VP



byproducts. We compared the morphology of pairs of miktoarm star terpolymers and their corresponding cyclic terpolymers and compared the sample morphology using transmission electron microscopy (TEM).<sup>29</sup>

Here, we exploit our prior synthetic approaches to make well-defined star and tadpole homo-/co-/terpolymers. The molecular characterization of all intermediate and final products was accomplished via size-exclusion chromatography (SEC) and proton nuclear magnetic resonance (<sup>1</sup>H NMR) spectroscopy. Small-angle X-ray scattering (SAXS) and TEM were employed to examine the solution cast and thermal-annealed bulk samples in order to gain insight into the role of the complex star and cyclic macromolecular architecture on the self-assembled microdomain morphologies.

## EXPERIMENTAL SECTION

**Materials.** Benzene (Sigma-Aldrich, 99%) was purified over CaH<sub>2</sub> and distilled under a high vacuum in a round bottom flask containing polystyryllithium oligomers [PS<sup>(-)</sup>Li<sup>(+)</sup>], exhibiting the characteristic orange color. Tetrahydrofuran (THF, Sigma-Aldrich, 99.9%) was refluxed over sodium, stirred in the presence of CaH<sub>2</sub> overnight, and distilled over Na/K alloy. Functionalized initiator 3-(*t*-butyldimethylsilyloxy)-1-propyllithium [FMC lithium (0.64 M in cyclohexane)] was diluted to the appropriate concentration with purified cyclohexane in a custom-made glass apparatus. *sec*-Butyllithium (*n*-BuLi, 1.4 M in cyclohexane, Sigma-Aldrich) was used without further purification and diluted with dry *n*-hexane. Isoprene (Sigma-Aldrich, 99%) was purified over CaH<sub>2</sub> and subsequent double distillation over *n*-BuLi under stirring for 30 min at 0 °C and stored in precalibrated ampoules. Styrene (St, Sigma-Aldrich, 99%) was purified by distillation over CaH<sub>2</sub> and subsequently over dibutylmagnesium (Sigma-Aldrich, 1 M solution in heptane) and stored in precalibrated ampoules. 2-Vinylpyridine (2-VP, Sigma-Aldrich, 97%) was distilled over CaH<sub>2</sub> and sodium mirror, stirred in the presence of trimethylaluminum (Sigma-Aldrich, 97%) at 0 °C, and used directly for the polymerization. The linking agent methyltrichlorosilane (CH<sub>3</sub>SiCl<sub>3</sub>, Sigma-Aldrich, 99%) was purified by fractional distillation and stored in precalibrated ampoules. Methanol (Sigma-Aldrich, 99.8%) (terminating agent) was stored under a high vacuum and used as received. *N,N'*-Dicyclohexylcarbodiimide (DCC), 4-dimethylaminopyridine (DMAP), and PMDETA were used as received.

**Measurements.** The number average molecular weight ( $M_n$ ) and the polydispersity index ( $\mathcal{D}$ ) were determined by SEC equipped with an isocratic pump, Styragel HR2 and HR4 columns in series (300 × 8 mm), a refractive index detector, and THF as the eluent at a flow rate of 1 mL/min at 30 °C. The calibration was performed using PS ( $M_p$ : 370–4 220 000 g/mol) and PI standards ( $M_p$ : 1030–1 040 000 g/

mol). <sup>1</sup>H NMR spectroscopy measurements were carried out in chloroform-*d* (CDCl<sub>3</sub>) on a Bruker AV-600 spectrometer.

Five percent w/w solutions of all samples were prepared in chloroform (CHCl<sub>3</sub>) and left at ambient conditions for 6 days in order to form 1 mm thick films. The films were subsequently further annealed at 130 °C for 2 days in a vacuum oven. A Leica EM-UC7 ultra-cryomicrotome at -120 °C, equipped with a diamond knife, was used to cut 40–50 nm thin sections. The film sections were collected in 400 mesh copper grids and stained with osmium tetroxide (OsO<sub>4</sub>) for 4 h in order to increase the electron density of the PI domains. The samples containing P2VP blocks were additionally stained with iodine (I<sub>2</sub>) vapor at room temperature for 8 h. Bright-field images of stained sections were studied using both an FEI Tecnai electron microscope operated at 120 kV and a JEOL 1230 TEM system operated at 80 kV. SAXS experiments were performed at the 12-ID-C synchrotron station with an X-ray energy of 12 keV ( $\lambda = 0.103$  nm) at the Advanced Photon Source of Argonne National Laboratory. For SAXS experiments, the scattering vector was calibrated using a silver behenate standard. The X-ray patterns are presented in the form of intensity ( $I$ ) versus scattering vector magnitude  $|\vec{q}| = q = 4\pi\lambda^{-1} \sin(\theta/2)$ , where  $\theta$  is the scattering angle and  $\lambda$  is the radiation wavelength.

## RESULTS AND DISCUSSION

All tadpole homo-/co-/terpolymers were synthesized in four general steps: (i) synthesis of the corresponding 3-miktoarm star polymer using anionic polymerization and chlorosilane chemistry. The essential requirement is that two out of the three arms must bear *t*-butyldimethylsilyloxypropyl functional end-groups. (ii) Deprotection of the *t*-butyldimethyl silyl groups with tetra-*n*-butylammonium fluoride (TBAF) to introduce hydroxypropyl chain-ends. (iii) Esterification of the -OH groups with 4-pentynoic acid in the presence of DCC and DMAP to introduce alkynyl end-groups, and (iv) intramolecular Glaser coupling reaction between the two alkynyl groups in the presence of Cu(I)Br/PMDETA in pyridine, at room temperature, to produce the final tadpole polymers. The synthetic procedure of the novel 3-miktoarm star terpolymer consisting of PI, PS, and P2VP is given in Scheme 1.

All manipulations were performed using anionic polymerization by high-vacuum techniques and carried out in evacuated, *n*-BuLi-washed, and solvent-rinsed glass reactors equipped with break-seals for the addition of reagents and constrictions for the removal of aliquots.<sup>42</sup> In general, the synthetic approach for the preparation of the (PI)<sub>2</sub>-*b*-PS-*b*-P2VP 3-miktoarm star terpolymer involves the selective

substitution of the two chlorine atoms of DCMSDPE by titration with  $(\text{pg-PI}^-\text{Li}^+)$  (pg: protected group, *t*-butyldimethylsilyloxypropyl), addition of *s*-BuLi to the in-chain double bond, polymerization of St from the newly created anionic site to produce the third “living” arm and finally polymerization of 2VP, to afford the 3-miktoarm star terpolymer. The initial step of the synthetic procedure involves the complete replacement of the two chlorine atoms of DCMSDPE by the  $(\text{pg-PI}^-\text{Li}^+)$  (Figure S1). Then, the required amount of *s*-BuLi was added, and the color of the solution immediately changed from pale yellow to orange, indicating the formation of the intermediate  $(\text{pg-PI})_2\text{DPE}^-\text{Li}^+$ . Stoichiometry is a crucial parameter in order to avoid byproducts, and as can be seen in Figure 1C, after the addition of *s*-BuLi, the SEC trace of the “living” star is identical to the one given in Figure 1B.

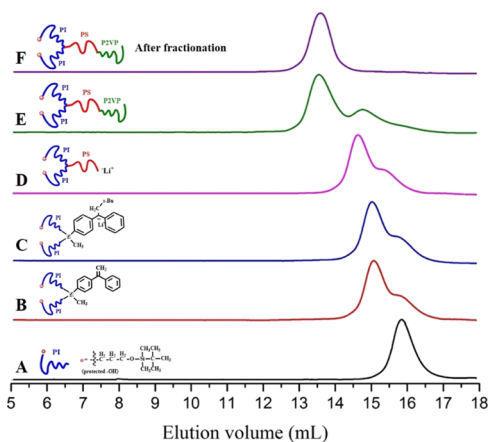


**Figure 1.** Monitoring the synthesis of the 3-miktoarm star terpolymer by SEC.

For the synthesis of the third block (PS), the desired amount of St was added to the in-chain “living” polymer  $[(\text{pg-PI})_2\text{DPE}^-\text{Li}^+]$  solution and the polymerization was left to completion at room temperature. After 16 h, a small aliquot was taken for SEC analysis. As seen in Figure 1D, the SEC trace shifted to a lower elution volume, indicating the formation of the  $(\text{pg-PI})_2\text{-}b\text{-PS}^-\text{Li}^+$  “living” 3-miktoarm star copolymer. In the final step of the synthetic procedure, benzene was removed under vacuum, freshly distilled THF was added, followed by introduction of an appropriate amount of 2-VP, under vigorous stirring, at  $-78\text{ }^\circ\text{C}$ . The polymerization was left to completion for 1 h, followed by addition of degassed methanol to quench the polymerization. As can be seen in Figure 1E, after polymerization of 2-VP, the SEC trace shifted to an even lower elution volume, indicating the formation of the 3-miktoarm star terpolymer. The small shoulder at the higher elution volume was eliminated by consecutive fractionations in a solvent/nonsolvent system. The SEC traces of all intermediate products, as well as of the final 3-miktoarm star terpolymer, exhibit narrow molecular weight distribution, indicating a high degree of homogeneity. The molecular characteristics of all intermediates, determined by SEC and  $^1\text{H}$  NMR, are shown in Table S1.

The next step for the preparation of the tadpole terpolymer was the removal of the *t*-butyldimethylsilyl protective groups in order to produce 3-miktoarm star terpolymer with hydroxypropyl chain-ends. Since treatment with concentrated

HCl of silicon containing star polymers produces arm cleavage,<sup>43</sup> TBAF was used for the deprotection of the  $-\text{OH}$  groups. The progress of the reaction was monitored by  $^1\text{H}$  NMR using the chemical shift of *t*-butylsilyl group at 0.9 ppm (Figure S2A). Treatment of the protected 3-miktoarm star terpolymer for 24 h with TBAF produces 100% hydroxypropyl chain-ends as proved by the disappearance of the chemical shift at 0.9 ppm (Figure S2B). To assure that there are no byproducts after removal of the *t*-butyldimethylsilyl end-groups, SEC analysis was performed again and showed identical SEC traces before and after deprotection. The deprotection details of the *t*-butylsilyl groups of the 3-miktoarm star homo-/copolymers are given in the Supporting Information with  $^1\text{H}$  NMR spectra in Figures S4B and S7B.

After the successful deprotection, the hydroxyl end-groups were esterified using an excess of 4-pentynoic acid in the presence of DCC and DMAP. Quantitative esterification was confirmed by the appearance of new chemical shifts at 2.2 and 2.5 ppm, which are attributed to the terminal proton of the alkyne groups and to the methylene protons adjacent to the triple bond, respectively. In addition, the chemical shifts corresponding to the proton near the hydroxyl group (proton b in the figure) after esterification indicate that all the hydroxyl groups have reacted (Figure S2C). The esterification details of the terminal hydroxyl end-groups of the 3-miktoarm star homo-/copolymers are given in the Supporting Information along with  $^1\text{H}$  NMR spectra in Figures S4C and S7C. The homodifunctional unimolecular ring closure between the two alkyne moieties was accomplished via the Glaser coupling reaction under high dilution, in the presence of  $\text{Cu}(\text{I})\text{Br}/\text{PMDETA}$  as catalyst and pyridine as solvent.<sup>44,45</sup> In order to minimize intermolecular polycondensation byproducts, a dilute solution of the dialkyne 3-miktoarm star terpolymer (7.5 mg/mL) was added dropwise slowly to the  $\text{CuBr}/\text{PMDETA}$  solution in pyridine. The oxidative alkyne dimerization was promoted by oxygen and led to the well-defined tadpole terpolymer with less than 5% polycondensation byproducts (the small shoulder at the lower elution volume), as seen in Figure 2B.

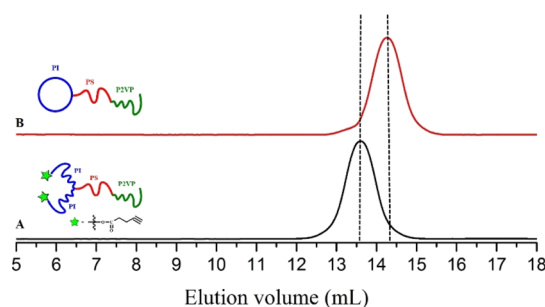


**Figure 2.** SEC traces of the (A) 3-miktoarm star terpolymer and (B) tadpole terpolymer.

Unambiguously, the SEC trace of the tadpole terpolymer after cyclization shifted to a higher elution volume, indicating smaller hydrodynamic volume compared to the corresponding 3-miktoarm star terpolymer. The *R* value (ratio of the apparent hydrodynamic molecular weight of the tadpole polymer to that of the corresponding star) is 0.77, indicating successful cyclization.<sup>46</sup> The difference of the apparent  $M_n$  between the tadpole terpolymer and the corresponding star, as calculated by SEC analysis, is evident in Table 1. The SEC traces of the

**Table 1. Molecular Characteristics of the 3-Miktoarm Star Terpolymer and the Corresponding Tadpole Terpolymer**

sample	$(\bar{M}_n)_{SEC}^a$ (g/mol)	$D^a$	$f_{(PI)}^b$ (% (w/w))	$f_{(PS)}^b$ (% (w/w))	$f_{(P2VP)}^b$ (% (w/w))	$f_{(PI)}^c$ % (v/v)	$f_{(PS)}^c$ % (v/v)	$f_{(P2VP)}^c$ % (v/v)
3- $\mu$ star terpolymer	61 000	1.06	0.36	0.27	0.37	0.40	0.27	0.33
tadpole terpolymer	47 400*	1.06	0.35	0.28	0.37	0.40	0.27	0.33

<sup>a</sup>SEC in THF at 35 °C using PS standards. <sup>b</sup>Mass fraction was calculated by <sup>1</sup>H NMR spectroscopy in CDCl<sub>3</sub> at 25 °C. <sup>c</sup>Densities used for calculation are of PI (0.92 g/cm<sup>3</sup>), PS (1.04 g/cm<sup>3</sup>), and P2VP(1.14 g/cm<sup>3</sup>). \* Apparent MW from GPC.

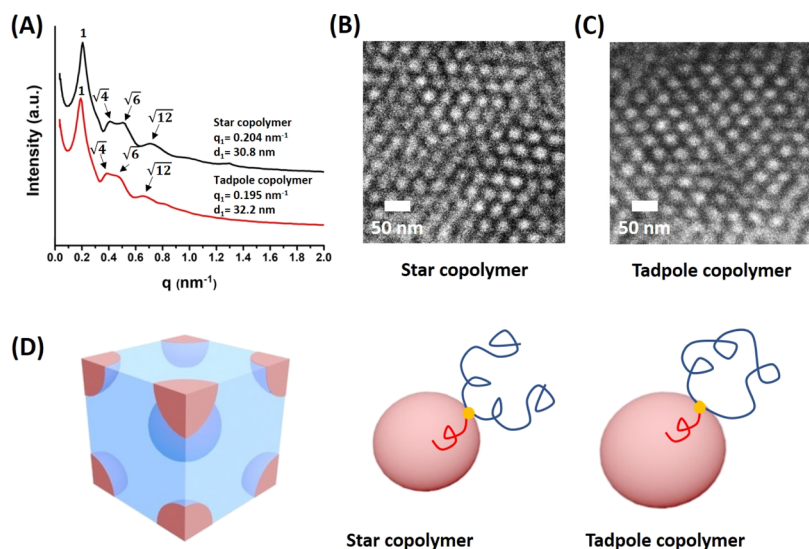


**Figure 3.** (A) SAXS patterns of the star and tadpole copolymers with the positions of the well-resolved Bragg peaks from a body-centered cubic (bcc) lattice indicated. The tadpole polymer has a larger lattice as evident from the slightly lower  $q$  position of the first (110) Bragg peak. (B) Bright-field TEM images of osmium-stained 3-miktoarm (PI)<sub>2</sub>-*b*-PS star copolymer and (C) (PI)<sub>2</sub>-*b*-PS tadpole copolymer showing the lighter spherical PS domains in the darker osmium-stained PI matrix. (D) Schematics of the bcc unit cell and chain packing for the star and tadpole spherical domains.

corresponding homo-/copolymers tadpoles can be seen in Figures S5 and S8. The molecular characteristics of the corresponding tadpoles are given in Tables S3 and S5.

Furthermore, the successful cyclization was also confirmed through the <sup>1</sup>H NMR analysis of the final tadpole terpolymer (Figure S2D). As a result of the Glaser coupling reaction and the formation of the 1,3-diyne, the chemical shift at 2.2 ppm (HC≡C-) completely disappeared in the spectrum of the tadpole terpolymer. The synthesis of the 3-miktoarm star homo-/copolymers is very well documented in the literature;<sup>47,48</sup> thus, the detailed analysis is given in Supporting Information (Figures S3 and S6).

The microdomain morphology of block polymers is sensitive to chain architecture, and our topological macromolecular isomers feature the additional packing constraints in determining the self-assembled morphologies. For example, by designing 4-miktoarm copolymers having two pairs of the asymmetric but inverse arm block sequence, it was possible to access a tricontinuous (i.e., double gyroid) morphology at an overall symmetric 50/50 volume fraction composition, where the linear diblock domain morphology is normally deep within the lamellar phase window.<sup>49</sup> The synthesis of miktoarm star terpolymers revealed unique 2D periodic highly non-constant mean curvature structures due to the requirement that the single junction connecting all three types of blocks must reside on lines, where domains of all three types of block meet, rather than be distributed over the intermaterial dividing surfaces between domains as is normally the case for linear blocks.<sup>50</sup>

In order to elucidate the bulk-state microdomain morphologies of the star and tadpole copolymer and terpolymer pairs, we employed SAXS and TEM. Samples of the star and tadpole copolymers (PI)<sub>2</sub>-*b*-PS and (PI)<sub>2</sub>-*b*-PS were cast from chloroform and annealed at 130 °C for 2 days and examined by SAXS (see Figure 3A). For both the star and tadpole architectures, the  $q/q_1$  ratios for the set of observed peaks (1,  $\sqrt{4}$ ,  $\sqrt{6}$ ,  $\sqrt{12}$ ) correspond to allowed reflections from a body-centered cubic (bcc) lattice, suggesting that the minority PS component has formed spherical domains in the majority PI matrix. Bright-field TEM images using OsO<sub>4</sub> to stain the PI chains are given in Figure 3B,C. Light, unstained spherical PS domains are ordered in the darker stained PI matrix. The lowest order SAXS reflection for bcc lattice is the (110) peak leading to a cubic lattice parameter of 43.6 nm for the star copolymer and 45.5 nm for the tadpole polymer. The center-to-center sphere distances along the body diagonal direction,  $\langle 111 \rangle$ , are 37.8 nm and 39.4 nm, respectively, consistent with the distances observed between columns of spheres in the TEM images where the projected image symmetry is approximately 6-fold (i.e. along the [111] projection). A schematic of the suggested chain packing is shown in Figure 3D. Because the two polymers have identical composition and volume fraction, the larger unit cell for the tadpole polymer means that the spherical domains are also larger, indicating a higher aggregation number for the tadpole over the star. The average number of star molecules forming a spherical domain is approximately 407, whereas for the tadpole polymer, the

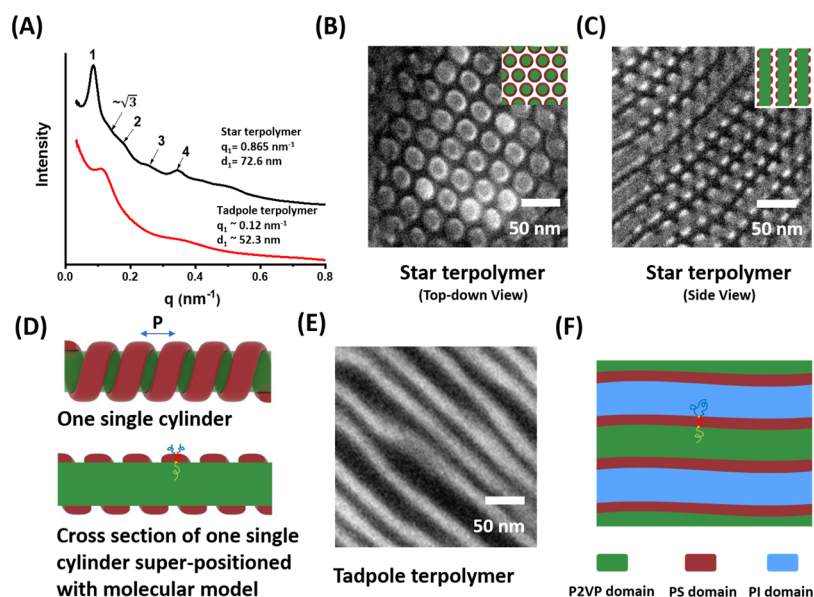


**Figure 4.** (A) SAXS patterns of the star and tadpole terpolymers with the positions of the lowest  $q$  peak and corresponding  $d$  spacing indicated. (B,C) Bright-field TEM images of osmium and iodine-stained 3-miktoarm  $(\text{PI})_2\text{-}b\text{-PS-}b\text{-P2VP}$  star terpolymer showing axial and transverse projections of the three-phase morphology. The unstained PS domains are the brightest, the  $\text{OsO}_4$ -stained PI matrix is the darkest, and the iodine-stained P2VP domains appear gray. (D) Schematics of the unit cell and chain packing in the star domains. The pitch of the PS helices is given by  $P$ . (E)  $(\text{PI})_3\text{-}b\text{-PS-}b\text{-P2VP}$  tadpole terpolymer. The unstained PS domains are bright while the darker domains are stained by osmium and iodine. (F) Schematics of the unit cell and chain packing in the tadpole domains. Transverse views of the three-component four-layer structure.

average spherical domain has 12% more molecules ( $\sim 456$ ). Based on the size and aggregation number for each type of PS spherical domain, the area/junction for the star molecule is  $4.2 \text{ nm}^2$  while that of the tadpole molecule is  $4.0 \text{ nm}^2$ .

Samples of the star and tadpole terpolymers  $(\text{PI})_2\text{-}b\text{-PS-}b\text{-P2VP}$  and  $(\text{PI})_3\text{-}b\text{-PS-}b\text{-P2VP}$  were also cast from chloroform and annealed at  $130 \text{ }^\circ\text{C}$  for 2 days and examined by SAXS (see Figure 4A). The star terpolymer exhibits a well-defined, strong, low angle peak ( $d = 72.6 \text{ nm}$ ) with several broader peaks at higher  $q$  with a  $q/q_1$  ratio of 1, 2, 3, 4 with a weak shoulder beyond the primary peak, near a position corresponding to  $\sqrt{3}$ . However, the scattering pattern from the tadpole shows only a single broad peak with a  $d$ -spacing of approximately  $53 \text{ nm}$ .

Bright-field TEM images of microtomed sections of the terpolymers were acquired using different staining protocols so as to visualize the individual types of domains to help decipher the morphologies. Figure S9A shows the star terpolymer stained with  $\text{I}_2$ , a stain specific to the P2VP domains. The field of view includes dark, hexagonally packed circular-shape domains as well as parallel dark striped domains that together indicate that the P2VP domains are cylindrical and packed on a 2D hexagonal lattice. Next, by using  $\text{OsO}_4$  as the stain, the PI block is targeted (Figure S9B). The PI block is the largest component block, and at 40 vol %, it likely forms the matrix. Some image regions show a 2D hexagonally packed array of light domains in a dark PI honeycomb pattern. As well, in other orientations, the PI phase appears as alternating dark parallel stripe regions having fine corrugations extending outward from the domain edges. When both the  $\text{I}_2$  and  $\text{OsO}_4$  stains are used, the TEM images show three distinct levels of contrast. A typical section displays features with hexagonal packing as well as parallel linear features (Figure 4B,C). The regions with hexagonal symmetry have a circular gray core region, surrounded by a thin, bright concentric ring embedded in the dark honeycomb matrix. The parallel features

appear as gray layers with alternating staggered and closely spaced, bright regions within an outer dark region. Taking all these features into account leads to the schematic model in Figure 4D, where hexagonally packed P2VP cylinders are wrapped by thinner, helically twisting PS belts embedded in a PI matrix. The PS domains appear to wrap around the P2VP cylinder as a single helical domain. The helical pitch of the belt-like PS domains is approximately  $45 \text{ nm}$ . Tomographic analysis is necessary to determine the handedness of the helical PS domains and to determine if there is axial registry between neighboring PS–P2VP domains. We note that helices with a single sense of twist would be frustrated when arranged on a hexagonal lattice. Because the electron density contrast is largest between the P2VP and PI components and these two blocks constitute the two largest volume fractions, the SAXS will be dominated by the hexagonally packed P2VP cylinders in the PI matrix, in agreement with the peaks identified in the SAXS pattern (Figure 4A).

Figures 4E and S10 show the  $(\text{PI})_3\text{-}b\text{-PS-}b\text{-P2VP}$  tadpole terpolymer stained with either  $\text{I}_2$  or  $\text{OsO}_4$  or with both stains. All bright-field TEM images show rather poorly ordered undulating layer-like structures with essentially two levels of contrast. No end-on views suggestive of cylinder-like domain packing were found. The large variation of the domain thicknesses is unexpected, and the basic 1D period (from SAXS) is considerably smaller than for the corresponding 2D periodic star terpolymer. Unlike the star and tadpole copolymer samples, both of which exhibit the same microdomain structure, the star and tadpole terpolymer samples exhibit dramatically different microdomain morphologies.

Sample morphology depends on many factors, especially composition, molecular weight, chain architecture, and the segregation strength between the various pairs of blocks. The segregation strength can be estimated from the respective molecular weights of the blocks and the  $\chi$  parameter or solubility parameter difference between the various pairs of

blocks. Using the solubility parameter differences for PI–PS 1.8 MPa<sup>1/2</sup>, PS–P2VP 2.3 MPa<sup>1/2</sup>, and PI–P2VP 4.1 MPa<sup>1/2</sup> and the degree of polymerization for each pair of blocks gives the segregation strengths as PI–PS 866 MPa<sup>1/2</sup>, PS–P2VP 858 MPa<sup>1/2</sup>, and PI–P2VP 2206 MPa<sup>1/2</sup>. Clearly, the strongest segregation is for the PI–P2VP pair. Thus, in the 2D periodic star terpolymer, the wrapped PS helices serve to partially shield direct contact of the P2VP and PI domains with some contact between the nonconnected end blocks of PI and P2VP in the regions between the PS helical domains. For higher PS content or perhaps for a linear terpolymer (a topological isomer), the PS may form a concentric cylindrical shell surrounding the central P2VP cylinder to prevent contact between the PI and P2VP blocks. In the tadpole, the terpolymer may prefer to adopt a four-layered –(P2VP–PS–PI–PS–P2VP)– repeat in order to eliminate the high interfacial energy contact between the PI and P2VP domains. Such a 1D periodic structure would have two thinner PS domains per repeat and the relative domain thicknesses P2VP–PS–PI–PS–P2VP would be in the ratio of ~0.33:0.27:0.8:0.27:0.33. Thus, for an osmium-stained sample, the expected layer repeat would be (P2VP–PS)<sub>light</sub>–PI<sub>dark</sub>–(P2VP–PS)<sub>light</sub>... and the layers would have relative thicknesses of 0.8 and 1.2, whereas for an iodine-stained sample, the layer repeat would be P2VP<sub>dark</sub>–(PS–PI–PS)<sub>light</sub>–P2VP<sub>dark</sub>... and the relative layer thicknesses would be 0.66 and 1.34 (approximately a 1:2 thickness ratio). The samples do not have a sufficient order in order to check these quantitative predictions, and further work is required.

Novel well-defined star and tadpole homo-/co-/terpolymers were synthesized by the combination of anionic polymerization, chlorosilane chemistry, and the Glaser coupling reaction. The synthesized 3-miktoarm star homo-/co-/terpolymers bear two arms with *t*-butyl-dimethylsilyloxypropyl functional end-groups, which after deprotection with TBAF and esterification with 4-pentynoic acid, were successfully transformed to alkyne end-groups. The cyclization between the two alkynyl moieties was feasible using the Glaser coupling reaction, under high dilution, in the presence of Cu(I)Br/PMDETA, using pyridine as solvent. As expected, the SEC traces of the tadpole polymers shifted to a higher elution volume compared to the corresponding 3-miktoarm star, indicating the successful cyclization. Furthermore, the detailed molecular characterization revealed the formation of tadpole polymers, in high yield without the existence of polycondensation byproducts. The self-assembled structures of the star copolymer and the star terpolymer as well as the tadpole copolymer and tadpole terpolymer were investigated by SAXS and TEM. Both the star and tadpole PI-*b*-PS copolymers displayed the same morphology, namely well-ordered spherical PS domains on a bcc lattice. Interestingly, the size of the spherical domains and the lattice constant of the tadpole polymer were larger than for the star copolymer, implying that the aggregation number depends on the chain architecture because the molecular weight, composition, and segregation strength of the two copolymer materials are essentially identical and the samples were prepared under the same processing protocol. However, in the case of the star and tadpole terpolymers, a structural phase transition was apparent. The PI–PS–P2VP star terpolymer assembled into a complex 2D periodic pattern composed of hexagonally packed P2VP cylinders, wrapped by PS helical domains in a PI matrix, while the tadpole terblock architecture resulted in a less well-ordered layered phase.

## ■ ASSOCIATED CONTENT

### Supporting Information

The Supporting Information is available free of charge on the ACS Publications website at DOI: 10.1021/acs.macromol.9b01013.

Synthesis of 3-miktoarm star terpolymer, synthesis of 3-miktoarm star homopolymer, synthesis of 3-miktoarm star copolymer, synthesis of tadpole copolymer, assembly analysis calculation, and supplementary TEM images (PDF)

## ■ AUTHOR INFORMATION

### Corresponding Authors

\*E-mail: [elt@rice.edu](mailto:elt@rice.edu). Phone +001-5087406061 (E.L.T).

\*E-mail: [Nikolaos.Hadjichristidis@kaust.edu.sa](mailto:Nikolaos.Hadjichristidis@kaust.edu.sa). Phone: +966-(0)12-8080789 (N.H).

### ORCID

George Polymeropoulos: 0000-0002-3352-0948

Panayiotis Bilalis: 0000-0002-5809-9643

Edwin L. Thomas: 0000-0001-5911-6524

Yves Gnanou: 0000-0001-6253-7856

Nikos Hadjichristidis: 0000-0003-1442-1714

### Notes

The authors declare no competing financial interest.

## ■ ACKNOWLEDGMENTS

The research reported in this publication was supported by the King Abdullah University of Science and Technology (KAUST) and the National Science Foundation under the Division of Materials Research Polymers Program grant # 1742864. This research used resources of the Advanced Photon Source, a U.S. Department of Energy (DOE) Office of Science User Facility operated for the DOE Office of Science by Argonne National Laboratory under contract no. DE-AC02-06CH11357.

## ■ REFERENCES

- (1) Szwarc, M. "Living" Polymers. *Nature* **1956**, *178*, 1168.
- (2) Polymeropoulos, G.; Zapsas, G.; Ntetsikas, K.; Bilalis, P.; Gnanou, Y.; Hadjichristidis, N. 50th Anniversary Perspective: Polymers with Complex Architectures. *Macromolecules* **2017**, *50*, 1253–1290.
- (3) Hadjichristidis, N.; Pispas, S.; Pitsikalis, M.; Iatrou, H.; Vlahos, C. Asymmetric star polymers: synthesis and properties. *Branched Polymers I*; Springer: Berlin, 1999; pp 71–127.
- (4) Hadjichristidis, N.; Pitsikalis, M.; Pispas, S.; Iatrou, H. Polymers with Complex Architecture by Living Anionic Polymerization. *Chem. Rev.* **2001**, *101*, 3747–3792.
- (5) Kim, Y.; Webster, O. *Star and Hyperbranched Polymers*; Mishra, M. K., Kobayashi, S., Eds.; Marcel Dekker: New York, 1999.
- (6) Mavroudis, A.; Hadjichristidis, N. Synthesis of Well-Defined 4-Miktoarm Star Quarterpolymers (4μ-SIDV) with Four Incompatible Arms: Polystyrene (S), Polyisoprene-1,4 (I), Poly(dimethylsiloxane) (D), and Poly(2-vinylpyridine) (V). *Macromolecules* **2006**, *39*, 535–540.
- (7) Hadjichristidis, N.; Fetters, L. J. Star-branched polymers. 4. Synthesis of 18-arm polyisoprenes. *Macromolecules* **1980**, *13*, 191–193.
- (8) Hadjichristidis, N.; Guyot, A.; Fetters, L. J. Star-Branched Polymers. 1. The Synthesis of Star Polyisoprenes Using Octa- and Dodecachlorosilanes as Linking Agents. *Macromolecules* **1978**, *11*, 668–672.

- (9) Hadjichristidis, N.; Roovers, J. E. L. Synthesis and solution properties of linear, four-branched, and six-branched star polyisoprenes. *J. Polym. Sci., Part B: Polym. Phys.* **1974**, *12*, 2521–2533.
- (10) Rahman, M. S.; Lee, H.; Chen, X.; Chang, T.; Larson, R.; Mays, J. Model Branched Polymers: Synthesis and Characterization of Asymmetric H-Shaped Polybutadienes. *ACS Macro Lett.* **2012**, *1*, 537–540.
- (11) Christodoulou, S.; Driva, P.; Iatrou, H.; Hadjichristidis, N. Synthesis and Micellization Behavior of Janus H-Shaped A2BC2Terpolymers. *Macromolecules* **2008**, *41*, 2607–2615.
- (12) Jia, Z.; Monteiro, M. J. Cyclic polymers: methods and strategies. *J. Polym. Sci., Part A: Polym. Chem.* **2012**, *50*, 2085–2097.
- (13) Kricheldorf, H. R. Cyclic polymers: synthetic strategies and physical properties. *J. Polym. Sci., Part A: Polym. Chem.* **2010**, *48*, 251–284.
- (14) Laurent, B. A.; Grayson, S. M. Synthetic approaches for the preparation of cyclic polymers. *Chem. Soc. Rev.* **2009**, *38*, 2202–2213.
- (15) Tomalia, D. A.; Frechet, J. M. *Introduction to the Dendritic State*; Wiley Online Library, 2002.
- (16) Voit, B. I. Dendritic polymers: from aesthetic macromolecules to commercially interesting materials. *Acta Polym.* **1995**, *46*, 87–99.
- (17) Hadjichristidis, N.; Iatrou, H.; Pitsikalis, M.; Mays, J. Macromolecular architectures by living and controlled/living polymerizations. *Prog. Polym. Sci.* **2006**, *31*, 1068–1132.
- (18) Iatrou, H.; Mays, J. W.; Hadjichristidis, N. Regular Comb Polystyrenes and Graft Polyisoprene/Polystyrene Copolymers with Double Branches (“Centipedes”). Quality of (1,3-Phenylene)bis(3-methyl-1-phenylpentylidene)dilithium Initiator in the Presence of Polar Additives. *Macromolecules* **1998**, *31*, 6697–6701.
- (19) Gauthier, M.; Moeller, M. Uniform highly branched polymers by anionic grafting: arborescent graft polymers. *Macromolecules* **1991**, *24*, 4548–4553.
- (20) Deffieux, A.; Borsali, R. Controlled synthesis and properties of cyclic polymers. *Macromolecular Engineering: Precise Synthesis, Materials Properties, Applications*; John Wiley & Sons, 2007; pp 875–908.
- (21) Chang, Y. A.; Waymouth, R. M. Recent progress on the synthesis of cyclic polymers via ring-expansion strategies. *J. Polym. Sci., Part A: Polym. Chem.* **2017**, *55*, 2892–2902.
- (22) Boydston, A. J.; Holcombe, T. W.; Unruh, D. A.; Fréchet, J. M. J.; Grubbs, R. H. A direct route to cyclic organic nanostructures via ring-expansion metathesis polymerization of a dendronized macro-monomer. *J. Am. Chem. Soc.* **2009**, *131*, 5388–5389.
- (23) Josse, T.; De Winter, J.; Gerbaux, P.; Coulembier, O. Cyclic Polymers by Ring-Closure Strategies. *Angew. Chem., Int. Ed.* **2016**, *55*, 13944–13958.
- (24) Quirk, R. P.; Wang, S.-F.; Foster, M. D.; Wesdemiotis, C.; Yol, A. M. Synthesis of cyclic polystyrenes using living anionic polymerization and metathesis ring-closure. *Macromolecules* **2011**, *44*, 7538–7545.
- (25) Laurent, B. A.; Grayson, S. M. Synthesis of cyclic amphiphilic homopolymers and their potential application as polymeric micelles. *Polym. Chem.* **2012**, *3*, 1846–1855.
- (26) Roovers, J.; Toporowski, P. M. Synthesis of high molecular weight ring polystyrenes. *Macromolecules* **1983**, *16*, 843–849.
- (27) Touris, A.; Hadjichristidis, N. Cyclic and Multiblock Polystyrene-block-polyisoprene Copolymers by Combining Anionic Polymerization and Azide/Alkyne “Click” Chemistry. *Macromolecules* **2011**, *44*, 1969–1976.
- (28) Lecommandoux, S.; Borsali, R.; Schappacher, M.; Deffieux, A.; Narayanan, T.; Rochas, C. Microphase Separation of Linear and Cyclic Block Copolymers Poly(styrene-*b*-isoprene): SAXS Experiments. *Macromolecules* **2004**, *37*, 1843–1848.
- (29) Polymeropoulos, G.; Bilalis, P.; Hadjichristidis, N. Well-defined cyclic triblock terpolymers: a missing piece of the morphology puzzle. *ACS Macro Lett.* **2016**, *5*, 1242–1246.
- (30) Pantazis, D.; Schulz, D. N.; Hadjichristidis, N. Synthesis of a model cyclic triblock terpolymer of styrene, isoprene, and methyl methacrylate. *J. Polym. Sci., Part A: Polym. Chem.* **2002**, *40*, 1476–1483.
- (31) Jiang, Y.; Zhang, Z.; Wang, D.; Hadjichristidis, N. An Efficient and General Strategy toward the Synthesis of Polyethylene-Based Cyclic Polymers. *Macromolecules* **2018**, *51*, 3193–3202.
- (32) Alkayal, N.; Zhang, Z.; Bilalis, P.; Gnanou, Y.; Hadjichristidis, N. Polyethylene-Based Tadpole Copolymers. *Macromol. Chem. Phys.* **2017**, *218*, 1600568.
- (33) Li, H.; Riva, R.; Jérôme, R.; Lecomte, P. Combination of Ring-Opening Polymerization and “Click” Chemistry for the Synthesis of an Amphiphilic Tadpole-Shaped Poly( $\epsilon$ -Caprolactone) Grafted by PEO. *Macromolecules* **2007**, *40*, 824–831.
- (34) Zhao, J.; Zhou, Y.; Li, Y.; Pan, X.; Zhang, W.; Zhou, N.; Zhang, K.; Zhang, Z.; Zhu, X. Modular construction of macrocycle-based topological polymers via high-efficient thiol chemistry. *Polym. Chem.* **2015**, *6*, 2879–2891.
- (35) Zhao, Z.; Zhu, Q.; Wang, Z.; Lu, J.; Jin, Z.; Liu, H. A Dicyclic Scaffold for Programmed Monocyclic and Polycyclic Polymer Architectures. *Macromolecules* **2017**, *50*, 8907–8915.
- (36) Tomikawa, Y.; Yamamoto, T.; Tezuka, Y. Construction of Hybrid-Multicyclic Polymer Topologies Composed of Dicyclic Structure Units by Means of An ESA-CF/Click-Linking Protocol. *Macromolecules* **2016**, *49*, 4076–4087.
- (37) Jia, Z.; Lonsdale, D. E.; Kulis, J.; Monteiro, M. J. Construction of a 3-miktoarm star from cyclic polymers. *ACS Macro Lett.* **2012**, *1*, 780–783.
- (38) Lee, T.; Oh, J.; Jeong, J.; Jung, H.; Huh, J.; Chang, T.; Paik, H.-j. Figure-eight-shaped and cage-shaped cyclic polystyrenes. *Macromolecules* **2016**, *49*, 3672–3680.
- (39) Shi, G.-Y.; Pan, C.-Y. Synthesis of and Click Chemistry. *Macromol. Rapid Commun.* **2008**, *29*, 1672–1678.
- (40) Gavrilov, M.; Amir, F.; Kulis, J.; Hossain, M. D.; Jia, Z.; Monteiro, M. J. Densely Packed Multicyclic Polymers. *ACS Macro Lett.* **2017**, *6*, 1036–1041.
- (41) Hossain, M. D.; Valade, D.; Jia, Z.; Monteiro, M. J. Cyclic polystyrene topologies via RAFT and CuAAC. *Polym. Chem.* **2012**, *3*, 2986–2995.
- (42) Hadjichristidis, N.; Iatrou, H.; Pispas, S.; Pitsikalis, M. Anionic polymerization: high vacuum techniques. *J. Polym. Sci., Part A: Polym. Chem.* **2000**, *38*, 3211–3234.
- (43) Hwang, J.; Foster, M. D.; Quirk, R. P. Synthesis of 4-, 8-, 12-arm star-branched polybutadienes with three different chain-end functionalities using a functionalized initiator. *Polymer* **2004**, *45*, 873–880.
- (44) Zhang, Y.; Wang, G.; Huang, J. Synthesis of Macrocylic Poly(ethylene oxide) and Polystyrene via Glaser Coupling Reaction. *Macromolecules* **2010**, *43*, 10343–10347.
- (45) Li, J.; Jiang, H. Glaser coupling reaction in supercritical carbon dioxide. *Chem. Commun.* **1999**, *0*, 2369–2370.
- (46) Lepoittevin, B.; Dourges, M.-A.; Masure, M.; Hemery, P.; Baran, K.; Cramail, H. Synthesis and characterization of ring-shaped polystyrenes. *Macromolecules* **2000**, *33*, 8218–8224.
- (47) Iatrou, H.; Siakali-Kioulafa, E.; Hadjichristidis, N.; Roovers, J.; Mays, J. Hydrodynamic properties of model 3-miktoarm star copolymers. *J. Polym. Sci., Part B: Polym. Phys.* **1995**, *33*, 1925–1932.
- (48) Hadjichristidis, N.; Iatrou, H.; Behal, S. K.; Chludzinski, J. J.; Disko, M. M.; Garner, R. T.; Liang, K. S.; Lohse, D. J.; Milner, S. T. Morphology and miscibility of miktoarm styrene-diene copolymers and terpolymers. *Macromolecules* **1993**, *26*, 5812–5815.
- (49) Tselikas, Y.; Hadjichristidis, N.; Lescanec, R. L.; Honeker, C. C.; Wohlgemuth, M.; Thomas, E. L. Architecturally-induced tricontinuous cubic morphology in compositionally symmetric miktoarm starblock copolymers. *Macromolecules* **1996**, *29*, 3390–3396.
- (50) Sioula, S.; Hadjichristidis, N.; Thomas, E. L. Novel 2-dimensionally periodic non-constant mean curvature morphologies of 3-miktoarm star terpolymers of styrene, isoprene, and methyl methacrylate. *Macromolecules* **1998**, *31*, 5272–5277.